Supplementary InfromationMaterials

Cyano-bridged perovskite $[(CH_3)_3NOH]_2[KM(CN)_6]$,[M: Fe(III), Co(III)] for high-temperature multi-axial ferroelectric applications with enhanced thermal and nonlinear optical performance

Magdalena Rok, Agnieszka Ciżman, Bartosz Zarychta, Jan K. Zaręba, Monika Trzebiatowska, Mirosław Mączka, Alessandro Stroppa, Shurong Yuan, Anthony E. Phillips, Grażyna Bator

CAPTIONS OF FIGURES

CAPTIONS OF TABLES

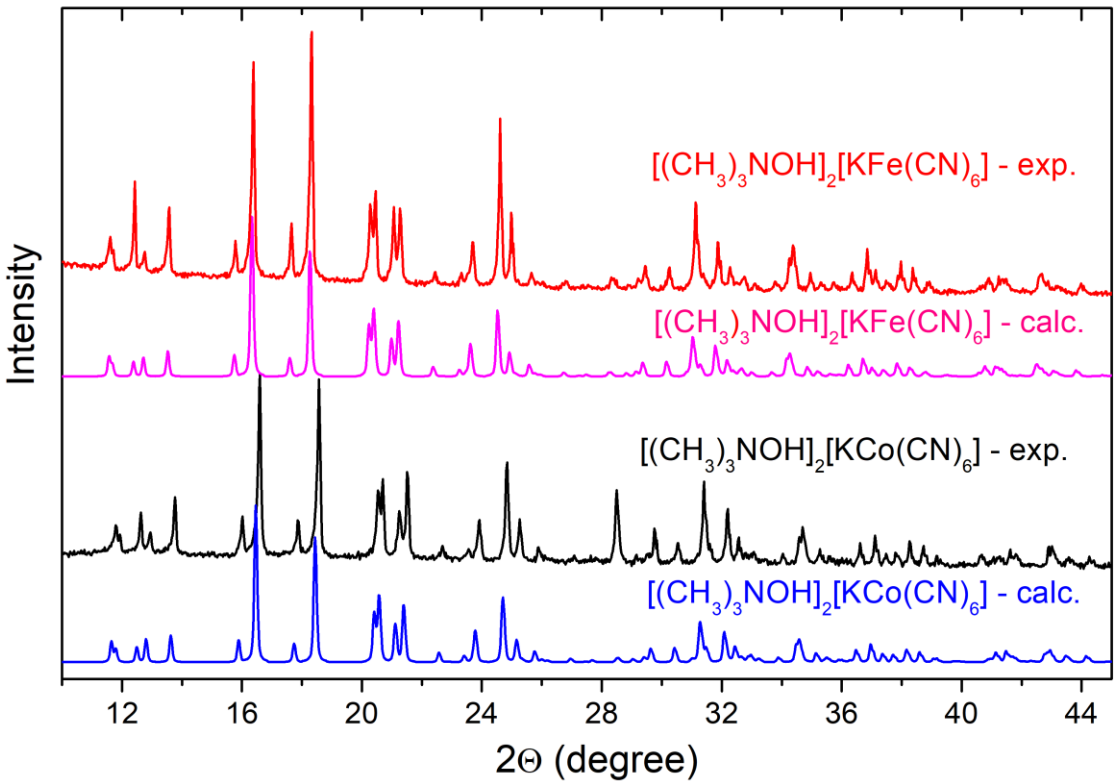

Fig. S1. X-ray diffraction pattern at 298 K of **TMAO-Co** (black) and calculated from crystal structure **TMAO-Fe** (red) presented in ref. [1]

(1) Xu, W. J.; Li, P. F.; Tang, Y. Y.; Zhang, W. X.; Xiong, R. G.; Chen, X. M. A Molecular Perovskite with Switchable Coordination Bonds for High-Temperature Multiaxial Ferroelectrics. *J. Am. Chem. Soc.* **2017**, *139*, 6369–6375.

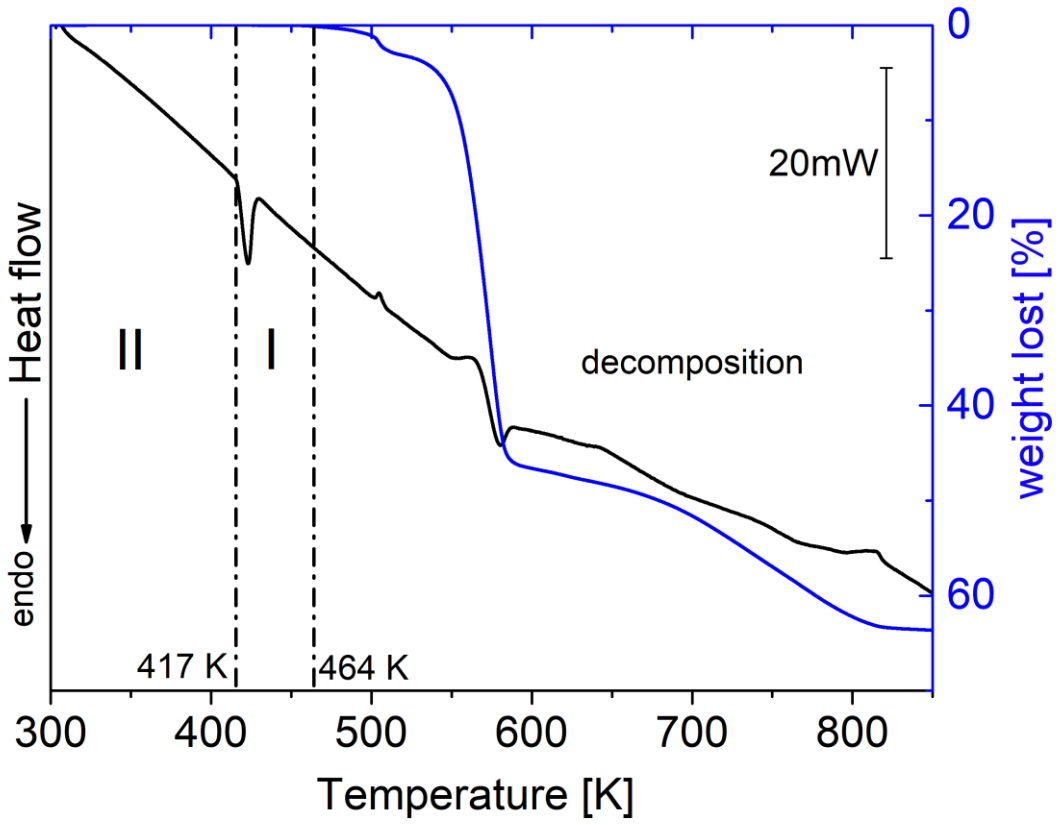

Fig. S2. The results of the simultaneous TGA/DSC analyses for **TMAO-Co** (sample mass m = 11.9960 mg, 5K/min.)

Table S1. Thermodynamic parameters of the phase transitions for **TMAO-Co.**

PT	**II → I**	
runs	cooling	heating
M [g/mol]	406.39	
T [K]	409	417
Δ*H* [J·g^{-1}]	71.5	75.5
Δ*H* [kJ·mol^{-1}]	29.1	30.7
Δ*S* [J·mol^{-1}·K^{-1}]	71.0	73.6

Table S2. Experimental details **TMAO-Co**.

	(II)	**(I)**
Crystal data		
Chemical formula	$C_{12}H_{20}CoKN_8O_2$	$C_{12}H_{20}CoKN_8O_2$
M_r	406.39	406.39
Crystal system, space group	Monoclinic, *Cc*	Cubic, $Fm\bar{3}m$
Temperature (K)	100.0(1)	440
a, *b*, *c* (Å)	15.1774 (9), 8.8150 (5), 14.3489 (9)	12.3427 (4), 12.3427 (4), 12.3427 (4)
α, β, γ (°)	90, 98.532 (6), 90	90, 90, 90
V (Å^3)	1898.5 (2)	1880.31 (18)
Z	4	4
Radiation type	Mo *K*α	Mo *K*α
μ (mm^{-1})	1.15	1.16
Crystal size (mm)	0.23 x 0.15 x 0.12	0.23 x 0.18 x 0.10
Data collection		
Diffractometer	Xcalibur CCD	
Absorption correction	SCALE3 ABSPACK	
min/max	0.5609/1.0000	0.7512/1.0000
No. of measured, independent and observed [$I > 2\sigma(I)$] reflections	6865, 2724, 2297	9110, 218, 121
R_{int}	0.064	0.041
$(\sin\theta/\lambda)_{max}$ (Å^{-1})	0.617	0.760
Refinement		
$R[F^2 > 2\sigma(F^2)]$, $wR(F^2)$, *S*	0.041, 0.095, 0.96	0.038, 0.108, 1.06
No. of reflections	2724	218
No. of parameters	224	22
No. of restraints	2	0
H-atom treatment	H atoms treated by a mixture of independent and constrained refinement	H-atom parameters constrained
$\Delta\rho_{max}$, $\Delta\rho_{min}$ (e Å^{-3})	0.38, −0.35	0.23, −0.18
Absolute structure	Classical Flack method preferred over Parsons because s.u. lower.	
Absolute structure parameter	0.11 (3)	

Computer programs: *SHELXL2013* (Sheldrick, 2013).

Table S3. Selected geometric parameters (Å, º) for **TMAO-Co**.

II - phase					
Bond	Experimental	Calculated	Bond	Experimental	Calculated
Co1—C2	1.885 (7)	1.8574	N5—C5	1.138 (9)	1.1758
Co1—C6	1.885 (8)	1.8581	N6—C6	1.155 (9)	1.1747
Co1—C4	1.899 (8)	1.8821	N10—O10	1.414 (9)	1.4323
Co1—C1	1.904 (8)	1.8827	N10—C10	1.484 (9)	1.4912
Co1—C3	1.906 (8)	1.8836	N10—C12	1.485 (9)	1.4921
Co1—C5	1.909 (8)	1.8821	N10—C11	1.503 (11)	1.4958
N1—C1	1.157 (10)	1.1741	N11—O11	1.431 (9)	1.4322
N1—K1	2.828 (8)	2.7961	N11—C14	1.477 (10)	1.4924
C2—N2	1.163 (9)	1.1743	N11—C15	1.479 (9)	1.4963
N3—C3	1.141 (10)	1.1752	N11—C13	1.493 (9)	1.4911
C4—N4	1.152 (9)	1.1760			
Angles	Experimental	Calculated	Angles	Experimental	Calculated
C2—Co1—C6	91.4 (3)	92.94	N3—C3—Co1	176.6 (7)	174.48
C2—Co1—C4	175.1 (3)	173.64	N4—C4—Co1	175.8 (7)	175.44
C6—Co1—C4	91.1 (3)	90.75	N5—C5—Co1	174.4 (7)	174.10
C2—Co1—C1	87.9 (3)	90.94	N6—C6—Co1	177.3 (7)	177.76
C6—Co1—C1	88.5 (3)	86.04	O10—N10—C10	110.0 (6)	105.57
C4—Co1—C1	88.0 (3)	94.48	O10—N10—C12	110.6 (7)	109.23
C2—Co1—C3	91.0 (3)	87.28	C10—N10—C12	110.9 (6)	110.36
C6—Co1—C3	86.9 (3)	88.75	O10—N10—C11	104.6 (6)	109.73
C4—Co1—C3	93.4 (3)	87.63	C10—N10—C11	109.5 (7)	110.55
C1—Co1—C3	175.2 (3)	174.40	C12—N10—C11	111.0 (6)	111.23
C2—Co1—C5	88.5 (3)	88.32	N10—O10—K1^{ix}	134.8 (4)	134.09
C6—Co1—C5	176.0 (3)	173.81	O11—N11—C14	104.2 (5)	109.20
C4—Co1—C5	89.2 (3)	88.56	O11—N11—C15	109.1 (6)	109.74
C1—Co1—C5	95.5 (3)	87.88	C14—N11—C15	111.7 (6)	111.50
C3—Co1—C5	89.1 (3)	97.36	O11—N11—C13	109.6 (6)	105.35
C1—N1—K1	168.0 (7)	150.55	C14—N11—C13	110.8 (6)	110.39
N1—C1—Co1	175.0 (7)	176.24	C15—N11—C13	111.1 (6)	110.47
N2—C2—Co1	178.1 (6)	177.82			
I phase					
Bond	Experimental		Bond	Experimental	
Co1—C1	1.911 (4)		N10—O10	1.36 (3)	
K1—N1	3.115 (3)		N10—C10	1.55 (3)	
N1—C1	1.145 (5)				
Angles	Experimental		Angles	Experimental	
C1—Co1—C1^{i}	90.0		N1^{iii}—K1—N1^{iv}	180.0	
C1—Co1—C1^{ii}	180.0		O10^{v}—N10—O10	119.6 (2)	
N1^{iii}—K1—N1	90.0		O10—N10—O10	117.98 (17)	

Symmetry code(s): (i) −*y*+3/2, −*z*+3/2, −*x*+1; (ii) −*x*+1, −*y*+2, −*z*+1; (iii) −*y*+1, −*z*+1, −*x*+1; (iv) *y*, *z*, *x*; (v) −*y*+1, *z*, −*x*+1.

Table S4. Selected hydrogen-bond parameters for **TMAO-Co**.

D—H···*A*	*D*—H (Å)	H···*A* (Å)	*D*···*A* (Å)	*D*—H···*A* (°)
		II-phase		
O10—H10A···N6	0.82	1.82	2.642 (8)	175.4
O11—H11A···N2	0.82	1.81	2.628 (8)	172.2
C13—H00O···N6^{i}	0.96	2.69	3.601 (10)	157.9
		I-phase		
C10—H10B···N1^{ii}	1.05	2.31	3.161 (13)	137.5

Symmetry code(s): (i) x, $-y+2$, $z-1/2$; (ii) $-y+1$, $-z+1$, $-x+1$.

a)

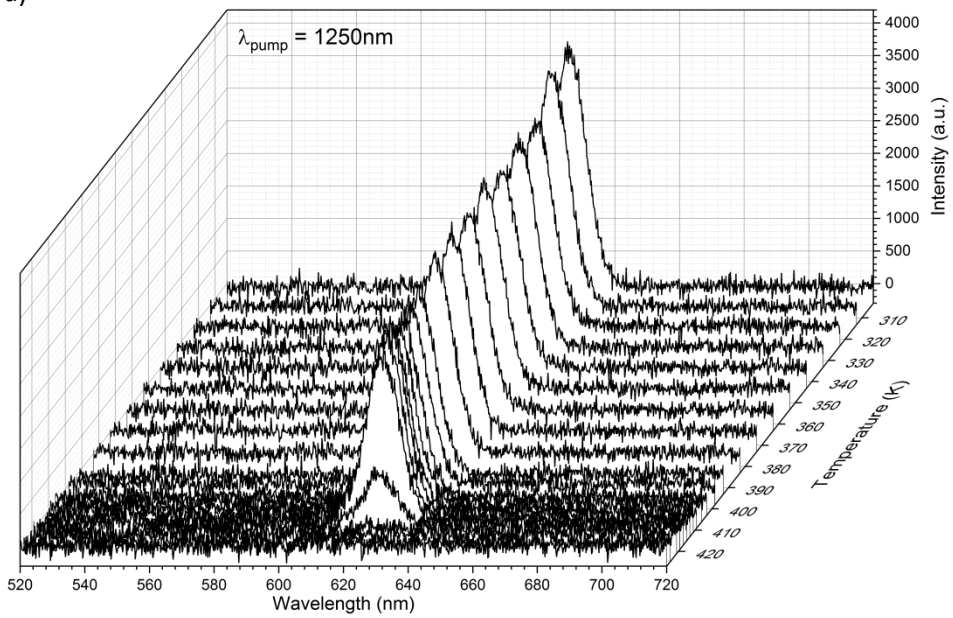

b)

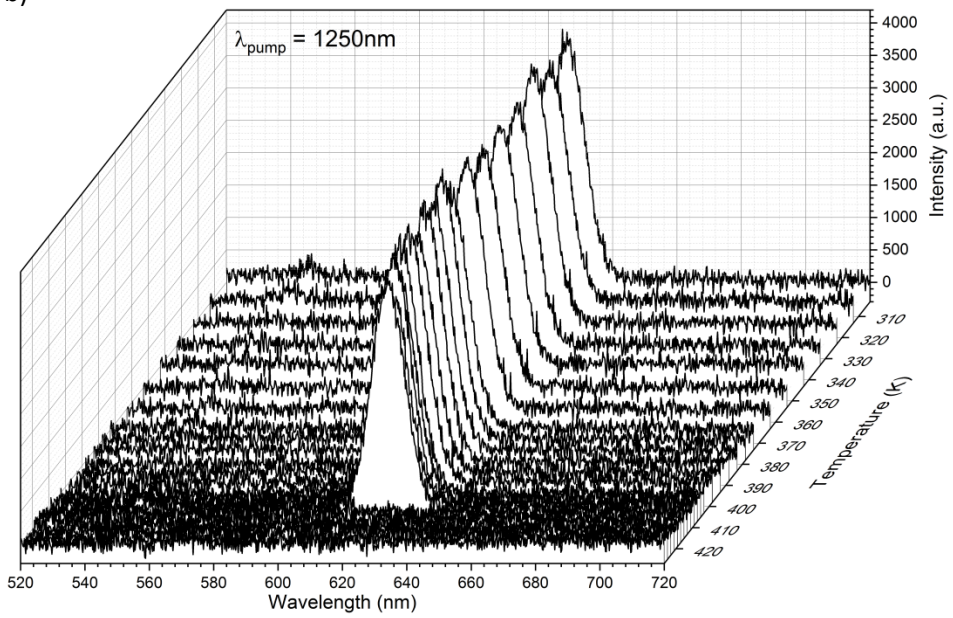

Fig. S3. Spectra obtained upon irradiation with the 1250 nm femtosecond laser pulses for **TMAO-Co** between 303K and 427K a) heating runs and b) cooling runs.

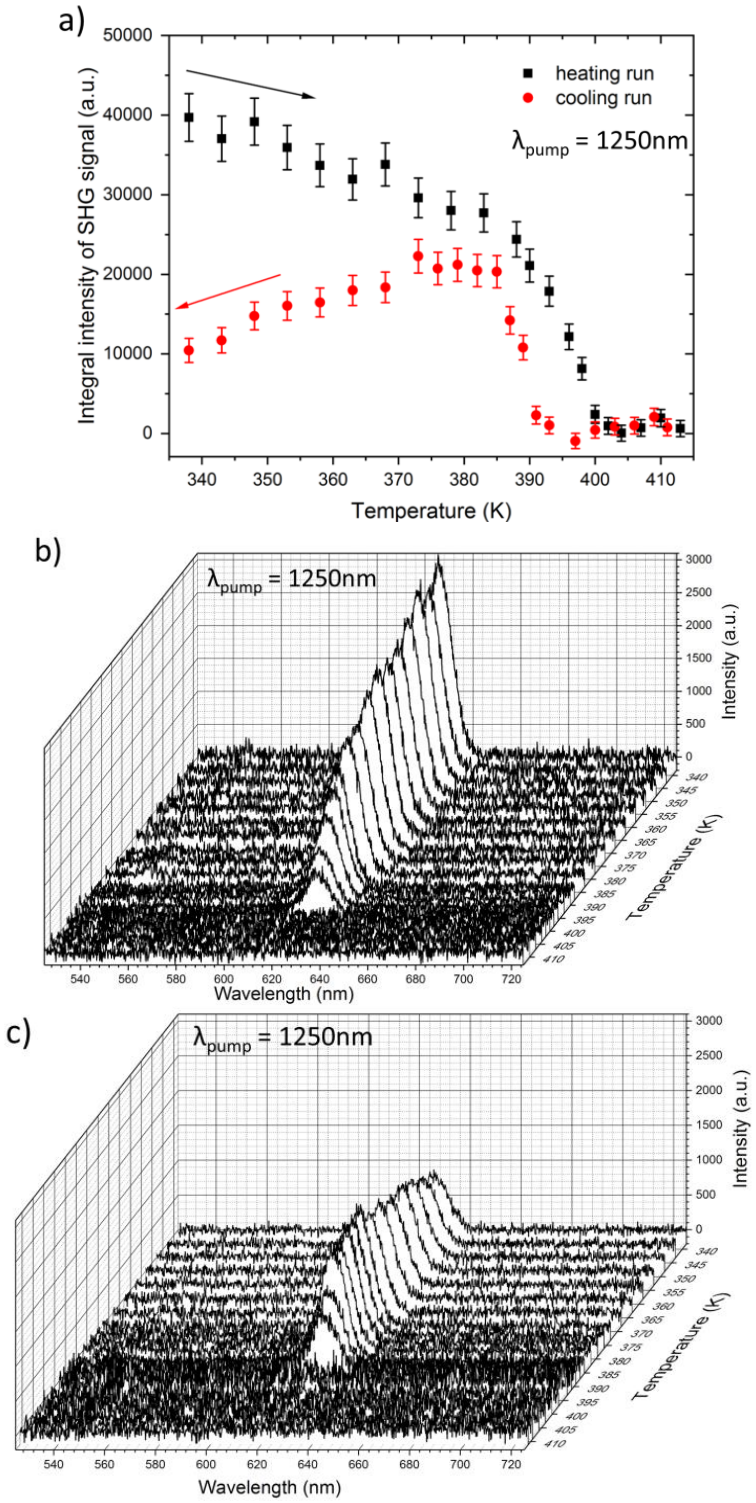

Fig. S4. a) Plots of integral intensity of SHG signal of **TMAO-Fe** for heating and cooling runs. b) Spectra obtained upon irradiation with 1250 nm femtosecond laser pulses of **TMAO-Fe** between 338 and 413 K on heating. c) Spectra obtained upon irradiation with 1250 nm femtosecond laser pulses of **TMAO-Fe** between 338 and 411 K on cooling.

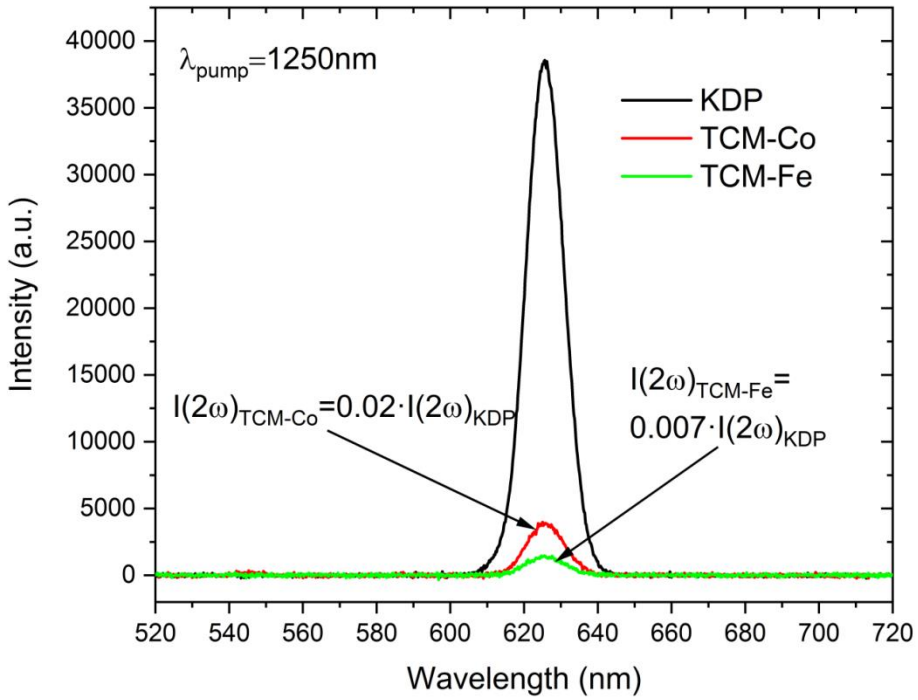

Fig. S5. SHG traces for **TMAO-Fe** (green), **TMAO-Co** (red) and that of KDP (black) obtained upon irradiation with 1250 nm femtosecond laser pulses. Signal collection time was equal to 6000 ms for **TMAO-Co** and **TMAO-Fe**, and 1200 ms for KDP; for clarity of presentation signal intensities are not normalized to the same integration time.

As noted in the main paper, in contrast with many molecular perovskites, **TMAO-Fe** undergoes a distinct "bond-switching" across its phase transition from the aristotype $Fm\bar{3}m$ structure. In the low-symmetry *Cc* phase, as well as the reference *C*2/*c* structure, some K···N-C-Fe links, which form the edges of the framework cage, break at the relatively ionic K···N bonds. The potassium and the nitrogen atoms re-connect through the -OH moiety of the A-site $TMAO^+$ cation, forming a new K···O-H···N-C-Fe edge of the framework cage. Therefore, when we perform functional group analysis, an equally valid alternative would be to consider the -OH group as part of the framework, leaving $(CH_3)_3N$··· alone as the A part. With this new separation formalism, we find that while the polarization along the *c*-axis stays almost unchanged, here the framework also contributes more than half of the polarization along the *a*-axis, while it has contributed little in the previous calculation. We can therefore further conclude that for the A-site $TMAO^+$ cation, the polarization along *a* comes roughly equally both from the trimethylammonium moiety and from the hydroxide group. Results from both sets of functional group analysis are presented in Table S5 below.

Table S5. Ferroelectric polarization of **TMAO-M**, calculated by DFT and a simple point-charge model. All values are given in units of μC cm^{-2}.

M			Berry phase			Point charge		
	Direction		*a*	*b*	*c*	*a*	*b*	*c*
Fe	**Total**		**0.937**	**0**	**0.732**	**2.367** **1.12***	**0**	**0.812** **0.54***
	Separately, where A=$[(CH_3)_3NOH]_2$ and BX_3=$KFe(CN)_6$	P_A	1.331	0	-0.124	2.733	0	-0.009
		P_{BX3}	-0.240	0	1.080	-0.596	0	0.677
		P_A+P_{BX3}	1.091	0	0.956	2.137	0	0.668
	Separately, where A=$[(CH_3)_3N]_2$ and BX_3=$(OH)_2KFe(CN)_6$	P_A	0.435	0	0.025	0.892	0	-0.177
		P_{BX3}	0.598	0	0.977	1.177	0	0.982
		P_A+P_{BX3}	1.033	0	1.002	2.069	0	0.805
Co	**Total**		**0.868**	**0**	**0.510**	**2.531**	**0**	**0.686**
	Separately, where A=$[(CH_3)_3NOH]_2$ and BX_3=$KCo(CN)_6$	P_A	1.384	0	-0.130	2.828	0	0.064
		P_{BX3}	-0.307	0	1.111	-0.310	0	0.683
		P_A+P_{BX3}	1.077	0	0.981	2.518	0	0.747
	Separately, where A=$[(CH_3)_3N]_2$ and BX_3=$(OH)_2KCo(CN)_6$	P_A	0.459	0	0.029	1.005	0	-0.195
		P_{BX3}	0.555	0	0.780	1.485	0	1.118
		P_A+P_{BX3}	1.014	0	0.809	2.490	0	0.923

*****result presented in ref.1

(1) Xu, W. J.; Li, P. F.; Tang, Y. Y.; Zhang, W. X.; Xiong, R. G.; Chen, X. M. A Molecular Perovskite with Switchable Coordination Bonds for High-Temperature Multiaxial Ferroelectrics. *J. Am. Chem. Soc.* **2017**, *139*, 6369–6375.

Table S6. Normal modes of **TMAO-M** compounds (M=Co, Fe) in the phase I (II). The IR-active modes are marked in red, the Raman-active-in blue, the modes active in both IR and Raman spectra are in green and the silent ones - in black.

Ion	Vibration	Free ion symmetry	Factor group symmetry
		O_h	O_h (C_s)
$M(CN)_6^-$	ν(CN)		
	ν_1	A_{1g}	A_{1g} (A'+A")
	ν_3	E_g	E_g (2A'+2A")
	ν_6	T_{1u}	T_{1u} (3A'+3A")
	ν(M-N)		
	ν_2	A_{1g}	A_{1g} (A'+A")
	ν_4	E_g	E_g (2A'+2A")
	ν_8	T_{1u}	T_{1u} (3A'+3A")
	δ(MCN)		
	ν_5	T_{1g}	T_{1g} (3A'+3A")
	ν_7	T_{1u}	T_{1u} (3A'+3A")
	ν_{10}	T_{2g}	T_{2g} (3A'+3A")
	ν_{12}	T_{2u}	T_{2u} (3A'+3A")
	δ(CMC)		
	ν_9	T_{1u}	T_{1u} (3A'+3A")
	ν_{11}	T_{2g}	T_{2g} (3A'+3A")
	ν_{13}	T_{2u}	T_{2u} (3A'+3A")
	T'		T_{1u} (3A'+3A")
	L		T_{1g} (3A'+3A")
$(CH_3)_3NOH^+$	T'		T_{1u} (3A'+3A")
	L		T_{1g} (3A'+3A")
K^+	T'		T_{1u} (3A'+3A")
	L		T_{1g} (3A'+3A")

Table S7. The room-temperature FT-IR and FT-Raman modes (in cm^{-1}) of **TMAO-M**, where M=Co, Fe, and their proposed assignment. The modes involving vibrations of CN^- ions are denoted by red color.

TMAO-Co		TMAO-Fe		Assignment
IR	Raman	IR	Raman	
3118w,b		3118w,b		νOH
3062m	3063m	3061m	3060m	νCH
3053m	3052w	3051m		νCH
3045sh	3045m	3045sh	3045m	νCH
3036w	3038w	3037w	3038w	νCH
2968vw	2977m	2968vw	2977m	νCH
	2956m		2956m	νCH
	2870w		2870w	overtone
2825m,b		2824m,b		νOH
	2805w		2804w	overtone
	2794w		2795w	overtone
2697m,b		2695s,b		νOH
2583s,b		2582s,b		νOH
	2530vw,b		2518vw,b	νOH
2474m	2475vw,b	2473m	2473vw,b	νOH
2153m	2153vs	2137s	2136vs	$\nu CN(\nu_1)$
2140s	2138vs	2129s	2128vs	$\nu CN(\nu_3)$
2130sh		2118sh		$\nu CN(\nu_6)$
2126vs	2126m	2114vs	2114m	$\nu CN(\nu_6)$
		2111sh		$\nu CN(\nu_6)$
2095vw		2084vw	2084vw	overtone
2090vw	2090vw	2081vw	2080vw	overtone
2082vw	2082vw	2070vw	2070vw	overtone
1638m,b		1640m,b		δOH
1555s		1557s		δOH
1544s		1545s		δOH
1480s	1483vw	1480s	1485vw	δCH_3
1460s		1455s		δCH_3
1449m	1450m	1446sh	1451m	δCH_3
1442s	1443m	1443s	1443m	δCH_3
1422w	1423vw	1421w	1422vw	δCH_3
1402m	1403w	1403m	1403w	δCH_3
1396w				δCH_3
1269w	1269vw	1269w	1270vw	ρCH_3
1255s	1255mw	1255s	1255vw	ρCH_3
1127w	1127w	1127w	1126w	ρCH_3
1124w		1124w		ρCH_3
951s	952m	951s	951m	νNO
941w	941m	942w	941m	νCN
896vw				overtone
858m		859		γOH
833s		834s		γOH

754w	755m	756w	756m	νCN
748sh	748sh	746sh	747sh	νCN
561m	557vw	522w		ρNO
515w	514w	511w	510w	ρNO
	501vw		501vw	δMCN(ν_7)
486w	485w	487w	485w	Skeletal def.
457w	459w	457m	459w	Skeletal def.
447sh	447vw		441vw	Skeletal def.
442w	441vw		428sh	Skeletal def.
430m	428w	421s	419vw	δMCN(ν_{10})
419s				δMCN(ν_{10})
411m	409w		400w	δMCN(ν_{10})
	402sh		386sh	νMC(ν_2) +δCNC
	396m		376m	νMC(ν_2) +δCNC
	381w			νMC(ν_4) +δCNC
	376sh			νMC(ν_4) +δCNC
	197w		193w	τCH_3
	160sh		153sh	δCMC(ν_{11}) +lattice
	148m		141s	δCMC(ν_{11}) +lattice
	131sh		126sh	lattice

Table S8. The observed IR and Raman modes (in cm^{-1}) of **TMAO-Co** and their proposed assignment.

IR			Raman			**Assignment**
80 K	**280 K**	**430 K**	**80 K**	**280 K**	**430 K**	
		3433m				νOH
		3234s				νOH
3131w,b	3118w,b					νOH
3101w,b						νOH
3063w	3062m	3061w	3064m	3063m	3059sh	νCH
3053w	3053m	3052w	3056m	3057m	3051m	νCH
3045sh	3046sh		3047w	3048w		νCH
3034w	3036w		3038w	3038w		νCH
3026vw	3024vw		3035w			νCH
3008vw						νCH
2993vw	2991vw	2991vw				νCH
2971vw	2970vw	2972vw	2979m	2977m	2976m	νCH
			2970w			νCH
			2956m	2956m	2957sh	νCH
		2921w,b				νOH
			2867w	2869w	2880vw	overtone
2828m	2827m,b			2838vw		νOH
2816m						νOH
			2803w	2804w	2805vw	overtone
			2793w	2794w		overtone

2751w						νOH
2741w	2731sh					νOH
2703m	2695m,b					νOH
2590sh						νOH
2549s	2581s,b					νOH
2511m						νOH
2483s	2475s,b					νOH
2471sh						νOH
2157m	2153m		2156vs	2152vs	2136s	νCN(ν_1)
2142s	2139s		2141s	2138s	2124m	νCN(ν_3)
2133sh	2129sh		2133m			νCN(ν_6)
2129vs	2127vs	2114vs	2129m	2127m		νCN(ν_6)
1663m	1639m,b	1635vw,b				δOH
1623m						δOH
1566m	1551m					δOH
1551m	1544m	1498m,b				δOH
1481m	1480m	1485s	1484vw	1485vw		δCH_3
1461w	1458sh					δCH_3
1451m	1448sh					δCH_3
1441m	1443m	1445s	1441w	1442w	1445w	δCH_3
1419vw	1421vw		1420vw			δCH_3
1400w	1403w	1407w	1408vw	1401w	1403vw	δCH_3
			1400w			δCH_3
1273w	1269w		1272vw	1270vw		ρCH_3
1259m	1255m	1240m	1255vw	1254vw		ρCH_3
1128w	1127w	1123w	1127vw	1126w		ρCH_3
1124w	1123w					ρCH_3
954m	952m	954m	953m	951m	951w	νNO
951sh						νNO
944w	942m	936m	945w	943sh	934w	νCN
			938w			νCN
	896vw	890w				overtone
871m	858m		868vw			γOH
848m	835m		847vw			γOH
763vw			762w			νCN
756w	756w	761w	756m	755m	761w	νCN
746w	747w		746w	749sh	748sh	νCN
565w	561w	554w	564vw	560vw		ρNO
			504vw			δCoCN(ν_7)
			486vw	485vw	495vw	Skeletal def.
			459vw	459vw	456vw	Skeletal def.
			442w	441w		Skeletal def.
			430w	427w		δCoCN(ν_{10})
			413w	409w		δCoCN(ν_{10})
			405sh			νCoC(ν_2) +δCNC
			400m	397m	386m	νCoC(ν_2) +δCNC
			381w	381w		νCoC(ν_4) +δCNC
			342vw	341vw		δCoCN(ν_5)

	303vw			?
	290vw			?
	225vw			lattice
	211sh			τCH_3
	203w	197w		τCH_3
	170sh			$\delta CCoC(\nu_{11})$ +lattice
	164w	159sh		$\delta CCoC(\nu_{11})$ + lattice
	148m	148m	160m	$\delta CCoC(\nu_{11})$ + lattice
	129w	128sh		lattice
	86w	84w		lattice

Key: s-very strong, s-strong, m-medium, w-weak, vw-very weak, sh-shoulder; ν_s–symmetric stretching, ν_{as}-asymmetric stretching, δ-in-plane bending (scissoring), ρ-rocking, ω-wagging, τ-twisting (torsion), γ-out-of-plane bending, T–translation, L–libration.

Table S9. The observed IR modes (in cm^{-1}) of **TMAO-Fe** and their proposed assignment.

IR			Assignment
80 K	**280 K**	**390 K**	
		3428sh	νOH
		3228m	νOH
3133w,b	3120w,b	3150m	νOH
3107w,b			νOH
3060m	3060m	3059m	νCH
3053m	3050m	3050m	νCH
3049m			νCH
3042sh	3043sh		νCH
3033w	3035w		νCH
3008vw			νCH
2992vw		2985w	νCH
2970vw	2967vw	2955w	νCH
2916vw	2917vw	2923w	νCH
2830w	2824w		νOH
2818w			νOH
2733sh			νOH
2699m	2694m,b		νOH
2686m			νOH
2577sh	2572s,b		νOH
2538s			νOH
2483s	2475s,b		νOH
2468sh			νOH
2140s	2137s	2134w	$\nu CN(\nu_1)$
2132s	2129s	2126w	$\nu CN(\nu_3)$
2121m	2118sh	2113m	$\nu CN(\nu_3)$
2117vs	2115vs	2104s	$\nu CN(\nu_6)$
		2077m	$\nu CN(\nu_6)$
1661m	1639m,b	1666w,b	δOH
1621m			δOH
1567m	1557m		δOH

1553m	1546m	1549w	δOH
1481m	1480m	1479s	δCH_3
1461m	1460m	1463s	δCH_3
1441m	1441m	1445s	δCH_3
1419w	1422w		δCH_3
1401m	1403m	1404w	δCH_3
1272w	1269w		ρCH_3
1261m	1256m	1252w	ρCH_3
1245w		1241sh	ρCH_3
		1164vw	ρCH_3
1132vw			ρCH_3
1128vw	1127vw		ρCH_3
1125vw	1124sh	1125vw	ρCH_3
		1049w	ρCH_3
953s	952s	952m	νNO
950sh			νNO
944m	941m	940m	νCN
871m	859m	849sh	γOH
847m	837m	833m	γOH
757w	757w	757w	νCN
745vw	746vw	744vw	νCN

a)

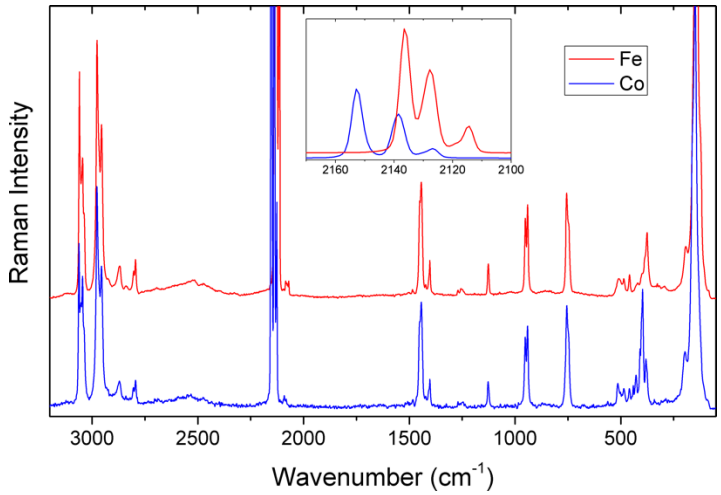

b)

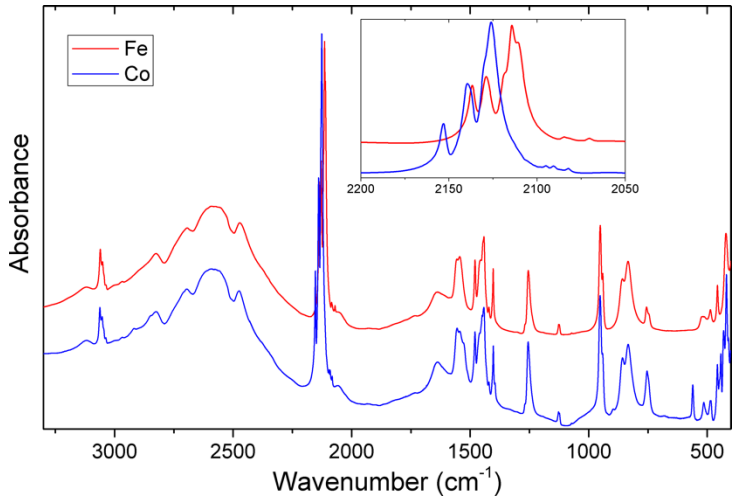

c)

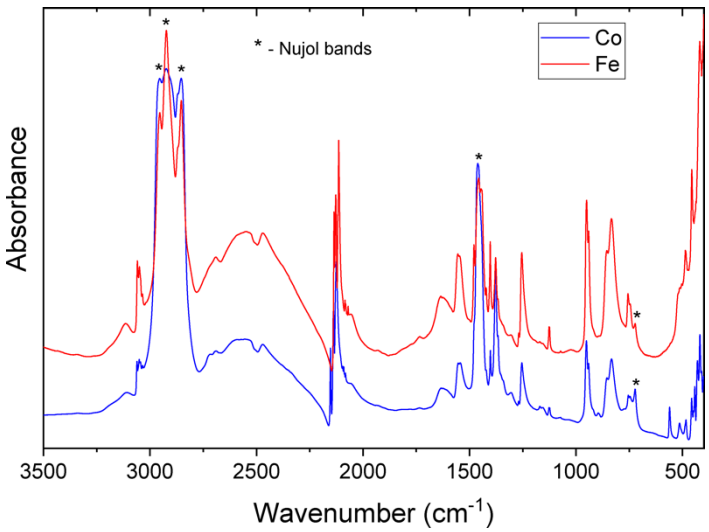

Fig. S6. a) The room-temperature FT-Raman spectra for **TMAO-Co** and **TMAO-Fe**. The insert shows the details of the most intense Raman bands. b) The room-temperature FT-IR spectra in KBr pellets and the 3300-400 cm^{-1} range. The insert shows the details of the most intense IR bands. c) The room-temperature FT-IR spectra of the studied compounds in Nujol mull and the 3300-400 cm^{-1} range. The asterisks denote Nujol bands.

a)

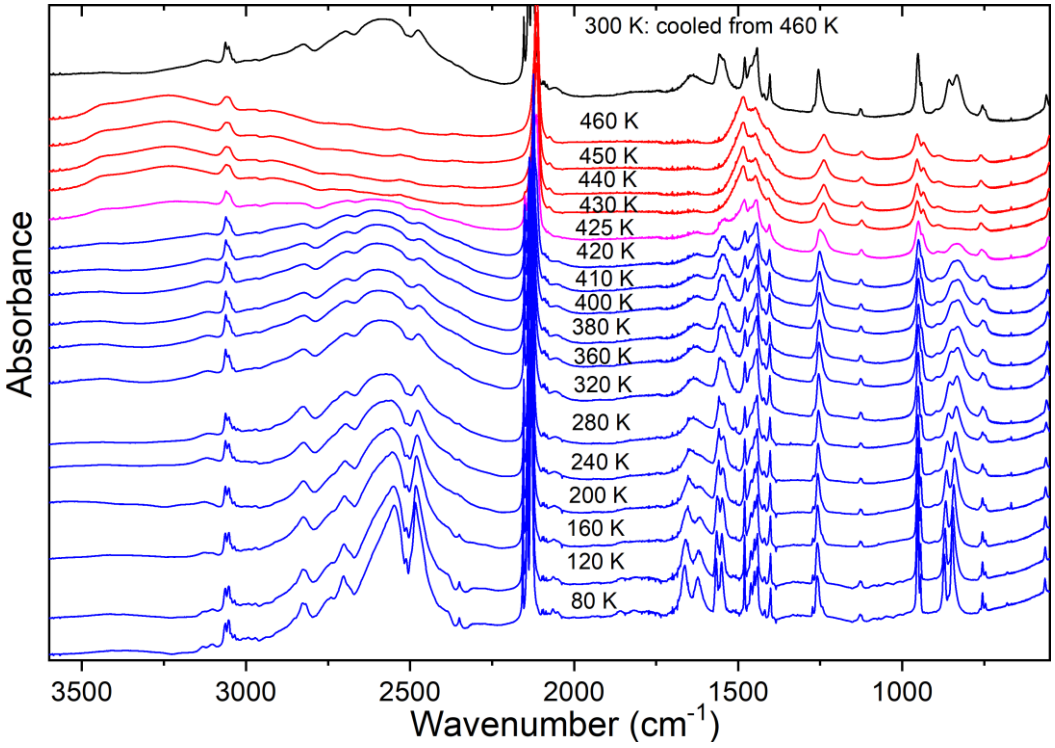

b)

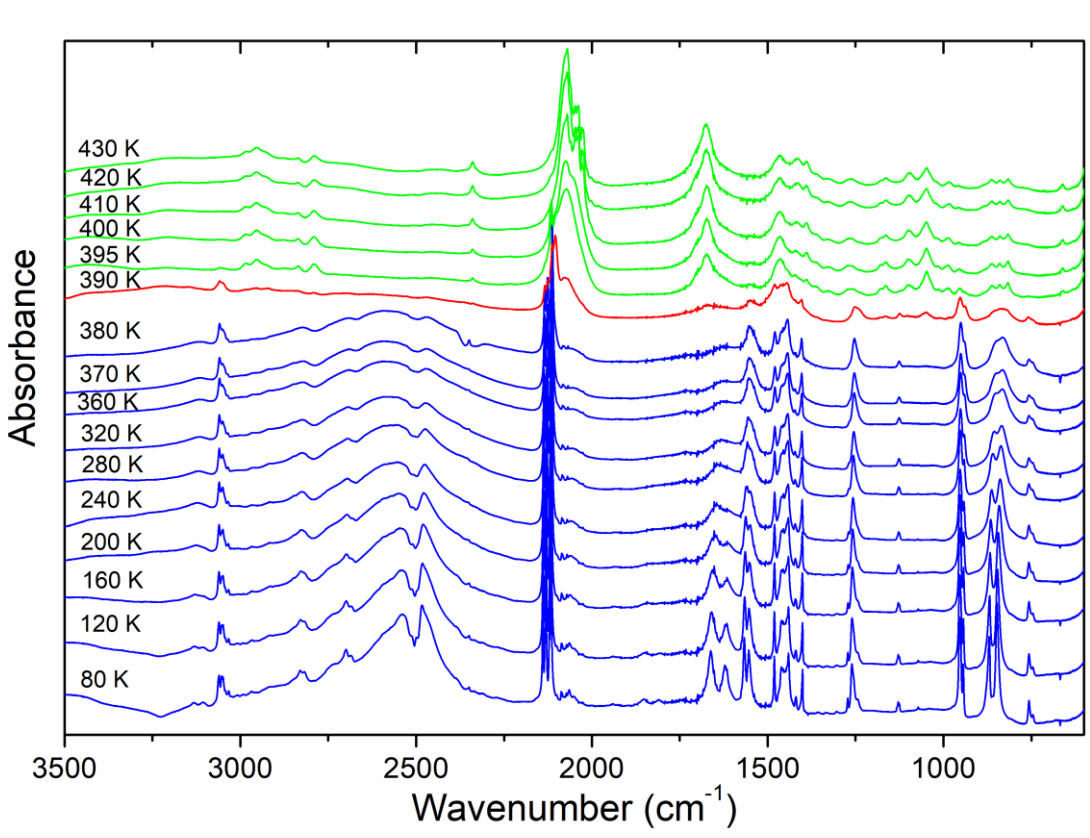

Fig. S7. The temperature-dependent IR spectra of a) **TMAO-Co** and b)**TMAO-Fe**.